# Long-Range Electric Field Control of Permalloy Layers in Strain-Coupled Composite Multiferroics

Michelle E. Jamer,[1] Colin R. Rementer,[2] Anthony Barra,[3] Alexander J. Grutter,[1] Kevin Fitzell,[2] Daniel B. Gopman,[4] Julie A. Borchers,[1] Gregory P. Carman,[3] Brian J. Kirby,[1,*] and Jane P. Chang[2]

[1] *NIST Center for Neutron Research, National Institute of Standards and Technology, Gaithersburg, Maryland 20899, USA*

[2] *Chemical and Biomolecular Engineering,University of California, Los Angeles, Los Angeles, California 90095, USA*

[3] *Mechanical and Aerospace Engineering, University of California, Los Angeles, Los Angeles, California 90095, USA*

[4] *Materials Science and Engineering Division, National Institute of Standards and Technology, Gaithersburg, Maryland 20899, USA*

(Received 2 April 2018; revised manuscript received 6 August 2018; published 18 October 2018)

Artificial composite multiferroic materials can be created by the interfacing of magnetostrictive and piezoelectric materials, allowing electric field control of magnetic properties. For multilayer-device applications, addition of weakly magnetostrictive layers is a potentially important means of tuning functionality. For such a device, the length scale over which weakly magnetostrictive layer(s) can be coupled to an applied electric field is of critical importance. In this work, we use polarized neutron reflectometry to characterize this distance for a model composite multiferroic multilayer system ($PbMg_{1/3}Nb_{2/3}O_3$-$PbTiO_3$/galfenol/permalloy). For a superlattice more than 100 nm thick, we observe that the magnetizations of all layers rotate coherently with the applied electric field. Further, we observe electric-field-induced rotation across the entirety of a 46-nm permalloy layer anchored by a single galfenol interface. The confirmation of long-range magnetic coupling in these strain-coupled multiferroic composites opens extensive opportunities for designer technological applications.

DOI: 10.1103/PhysRevApplied.10.044045

## I. INTRODUCTION

Strain-coupled composite multiferroic systems are attracting widespread interest to enable energy-efficient control of magnetism for numerous device applications, including radio-frequency resonators, sensors, and energy harvesters [1–3]. In principle, composite multiferroic systems offer a wide range of adaptability, as materials with different properties can be added to the composite to achieve the desired functionality. For example, magnetoelectric control of the highly magnetostrictive ferromagnet $Fe_{100-x}Ga_x$ (galfenol) [4] can be realized by the interfacing of it with piezoelectric $PbMg_{1/3}Nb_{2/3}O_3$-$PbTiO_3$ (PMN-PT) [5,6]. It has recently been shown that the magnetic properties of thin-film galfenol/PMN-PT composites can be further tuned through the addition of soft ferromagnetic layers with virtually zero magnetostriction [7]. Specifically, interfacing of galfenol with $Ni_{80}Fe_{20}$ (permalloy) layers significantly reduces the magnetic coercive field of the composite as a whole, an important consideration for high-frequency applications. In this case, electric field control of the weakly magnetostrictive component occurs through a secondary process: the applied electric field couples to the galfenol magnetization via strain, and then to the permalloy magnetization through ferromagnetic exchange. It is therefore important to establish the length scale over which a permalloy layer can be magnetoelectrically coupled. To that end, we use polarized-neutron reflectometry (PNR) to characterize the electric field response of the depth-dependent magnetization in galfenol/permalloy multilayer structures deposited on PMN-PT[011] substrates. These PNR investigations, in conjunction with micromagnetic calculations, reveal that the electric-field-induced magnetization rotation is uniform through the entire 100-nm thickness of a galfenol/permalloy superlattice and is nearly coherent throughout a galfenol/46-nm permalloy bilayer structure. The ability to couple essentially nonmagnetostrictive layer(s) to an electric field across such great distances provides a great deal of design flexibility, as it allows the addition of numerous distinct material layers to the multilayer stack to achieve the desired composite functionality.

*bkirby@nist.gov

 © 2018 American Physical Society

## II. SAMPLE FABRICATION

$Fe_{86}Ga_{14}/Ni_{80}Fe_{20}$ multilayers are deposited on piezoelectric $0.65[PbMg_{1/3}Nb_{2/3}O_3]$-$0.35[PbTiO_3]$ [011] substrates by room-temperature dc magnetron sputtering. The system base pressure is approximately $3 \times 10^{-5}$ Pa [7]. For all samples, the bottom sides of the substrates are coated with Au and Ti layers to allow "back-gating" of the applied voltage. The top surfaces of the substrates are then coated with an approximately-5-nm-thick Ti adhesion layer to attach an approximately-50-nm-thick Pt layer, which serves as a barrier to prevent an interfacial reaction between PMN-PT and the initial layer of galfenol. Magnetometry measurements of uniform films prepared by similar methods reveal that the magnetic coercive field is approximately a factor of 60 greater for galfenol (6 mT) than it is for permalloy (0.1 mT) [7]. For this work, we primarily consider two samples: a "superlattice" with layer structure [25-nm $Fe_{86}Ga_{14}$/6-nm $Ni_{80}Fe_{20}]_3$/25-nm $Fe_{86}Ga_{14}$, and a "bilayer" with structure 22-nm $Fe_{86}Ga_{14}$/46-nm $Ni_{80}Fe_{20}$.

The superlattice sample and the back-gating geometry are depicted in Fig. 1(a). An optical microscopy image of the superlattice sample is shown in Fig. 1(b). Because of the inherent roughness of the PMN-PT substrate, the surface topography is highly corrugated, with ridges separated by an average distance of $50 \pm 5$ $\mu$m, as determined with a stylus profilometer.

## III. BULK CHARACTERIZATION

Preliminary characterization of the voltage-strain-magnetization relationship for the superlattice sample is performed by Cu $K\alpha$ x-ray diffraction (XRD) and superconducting-quantum-interference-device (SQUID) magnetometry. Figure 1(c) shows the voltage dependence of the PMN-PT (022) reflection (i.e., growth-axis XRD scan) measured at room temperature. The left-hand peak corresponds to the $K\alpha_1$ reflection, while the right-hand shoulder corresponds to $K\alpha_2$ reflection. The substrate peaks monotonically shift to higher scattering angle $2\theta$ with increasing voltage, corresponding to a 0.08% increase in the $c$-axis lattice parameter at 400 V, as shown in the inset in Fig. 1(c). In-plane reflections are not probed for this work, but the voltage-dependent expansion of the PMN-PT growth axis is known to coincide with a lattice expansion along the in-plane $[01\bar{1}]$ axis and a corresponding contraction along the in-plane [100] axis [8].

The growth-axis XRD peaks for the superlattice sample are shown in Fig. 1(d). The galfenol (220) reflection does

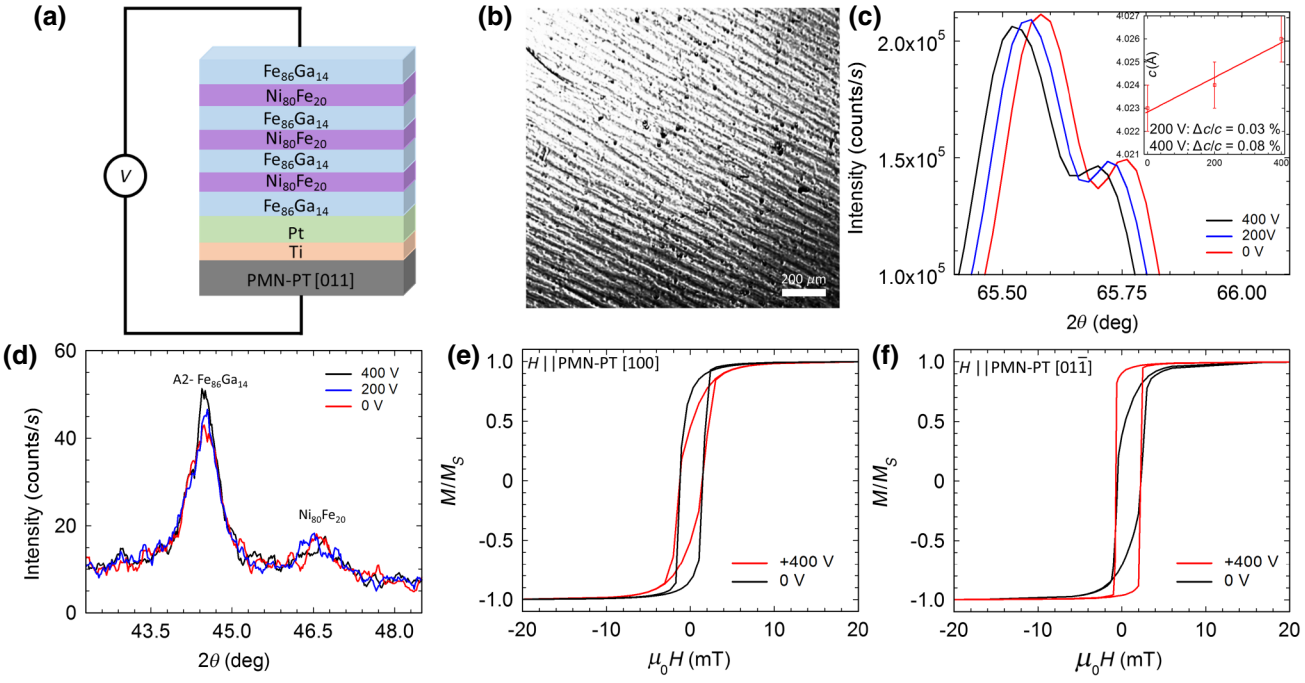


FIG. 1. Initial characterization of the superlattice sample. (a) Depiction of the layer structure. (b) Optical microscope image of the sample surface. The ridges correspond to a period of $50 \pm 5$ $\mu$m. (c) Voltage dependence of the PMN-PT (022) (growth-axis) x-ray reflection. The left and right peaks correspond to $K\alpha_1$ and $K\alpha_2$, respectively. The inset shows the corresponding change in $c$-axis lattice parameter with applied voltage. Error bars are derived from the angular reproducibility of the diffractometer. (d) Growth-axis XRD peak scans for the superlattice sample. No discernible voltage-dependent shifting is observed. (e),(f) Voltage-dependent magnetic hysteresis loops measured in a SQUID magnetometer for the superlattice at room temperature for an in-plane magnetic field applied parallel to the [100] and $[01\bar{1}]$ sample directions.

show a very slight monotonic increase in peak intensity with increasing voltage, suggestive of increased grain alignment. However, we are insensitive to any voltage-dependent peak shift in either of the sample peaks that would demonstrate voltage-dependent expansion. While it is possible that changes in sample strain are masked by the reduced counting statistics and vastly increased width for these polycrystalline peaks, it is also conceivable that strain transfer occurs over only a fraction of the superlattice thickness before relaxing.

As galfenol exhibits positive magnetostriction, we expect strain coupling from PMN-PT to manifest itself as an increase in magnetic anisotropy along the direction of expansion. As shown in Figs. 1(e) and 1(f), magnetometry reveals this to be the case here. For an applied magnetic field $H$ oriented parallel to the compression axis [Fig. 1(e)], application of 400 V decreases the remanent magnetization and hardens the loop, while for $H$ applied parallel to the expansion axis, voltage increases the remanent magnetization and softens the loop. As such, we can confidently conclude that the magnetization of this superlattice sample is coupled to the applied electric field via strain.

## IV. PNR MEASUREMENTS

Depth-sensitive PNR measurements provide critical information regarding the uniformity of the electric-field-induced rotation of the magnetization through the nonmagnetostrictive permalloy layers. Specifically, PNR allows determination of the scattering-length-density (SLD) depth profile of thin films and multilayers [9]. The SLD can be expressed in terms of a nuclear component indicative of the sample's nuclear composition and a magnetic component that is proportional to the sample magnetization (M). For a complete PNR measurement, incident neutrons are polarized with magnetic moments oriented parallel (+) or antiparallel (−) to $H$ applied at the sample position, and the scattered beam is spin analyzed before detection. The non-spin-flip reflectivities ($R^{++}$ and $R^{--}$) provide sensitivity to the nuclear SLD and the component of the in-plane magnetic SLD parallel to $H$, while the spin-flip reflectivities ($R^{+-}$ and $R^{-+}$) are sensitive to the in-plane component of the magnetic SLD perpendicular to the $H$. PNR measurements on the superlattice and bilayer samples are conducted with the PBR beamline at the NIST Center for Neutron Research. The data shown here are corrected for background, imperfect beam polarization, and beam footprint. Model fitting is performed with the Refl1D software package [10].

The samples are magnetically saturated with a magnetic field applied along the in-plane PMN-PT [100] direction before reduction of the field to 1 mT (i.e., near remanence) for measurement with progressively increasing applied voltage. Figures 2(a)–2(c) show the voltage-dependent non-spin-flip and spin-flip reflectivities [11] for the superlattice. The two non-spin-flip reflectivities $R^{--}$ and $R^{++}$ are significantly different, indicative of large remanent magnetization parallel to $H$. Further, for both $R^{--}$ and $R^{++}$, we observe first- and second-order Bragg peaks indicative of the nuclear and magnetic contrast in the repeating-layer structure. Electric-field-dependent effects are most pronounced in the spin-flip channel, as Fig. 2(c) shows scattering that increases progressively with voltage. The data are simultaneously fitted to a single model that features a perfectly repeating multilayer structure convolved with Gaussian roughness [12]. For this model, we assume that the nuclear SLD (i.e., the composition) is voltage independent, and that the magnetization vector rotates coherently with voltage (i.e., the magnitude of the magnetic SLD is voltage independent). The values of $\phi_m$ for all the galfenol layers are assumed to be equal, as are the values of $\phi_m$ for all of the permalloy layers. Despite the simplicity of the model and the constraints applied, the resulting fits are excellent [solid lines in Figs. 2(a)–2(c)]. The corresponding best-fit SLD profiles are shown in Fig. 2(d). There is intermixing between the permalloy and galfenol layers, most evident by the peak nuclear SLD of the relatively thin permalloy layers, which falls short of the expected value [13] of $9.26 \times 10^{-4}$ nm$^{-2}$. Since the SLD at any given depth represents the average over the sample plane, interfacial intermixing is attributable to short-range interfacial roughness, atomic interdiffusion, and/or apparent interdiffusion associated with layer waviness [14]. However, the superlattice region is clearly modulated [evident even without model fitting from the Bragg peaks in Figs. 2(a) and 2(b)], demonstrating that the degree of any actual interdiffusion is relatively minor. The voltage dependence of the angle between the applied magnetic field and magnetization, $\phi_m$, for the galfenol and permalloy layers is shown in Fig. 2(e). In the absence of an electric field, the sample exhibits an easy axis near $\phi_m = 15^\circ$ [Fig. 2(e)] distinct from the PMN-PT [100] axis, evident by the presence of 0-V spin-flip scattering in Fig. 2(c). Within fitting uncertainty, the galfenol and permalloy layers display identical $\phi_m$ at each voltage, increasing from approximately 15° at 0 V to nearly 40° at 400 V. Such non-90° rotation has been observed in similar systems featuring a competition between "intrinsic" anisotropy and anisotropy induced by an electric field [15]. Treating the $\phi_m$ values for each of the galfenol and permalloy layers as separate, independent fitting parameters does not substantially improve the fit and results in values of $\phi_m$ comparable to those in Fig. 2(e). In addition, the data cannot be fit with models in which the $\phi_m$ values of the permalloy layers are held constant with voltage. Thus, the data are consistent with coherent magnetization rotation for all the galfenol and permalloy layers throughout the entire 100-nm superlattice stack on application of an electric field. Conversely, the data are inconsistent with reversal that

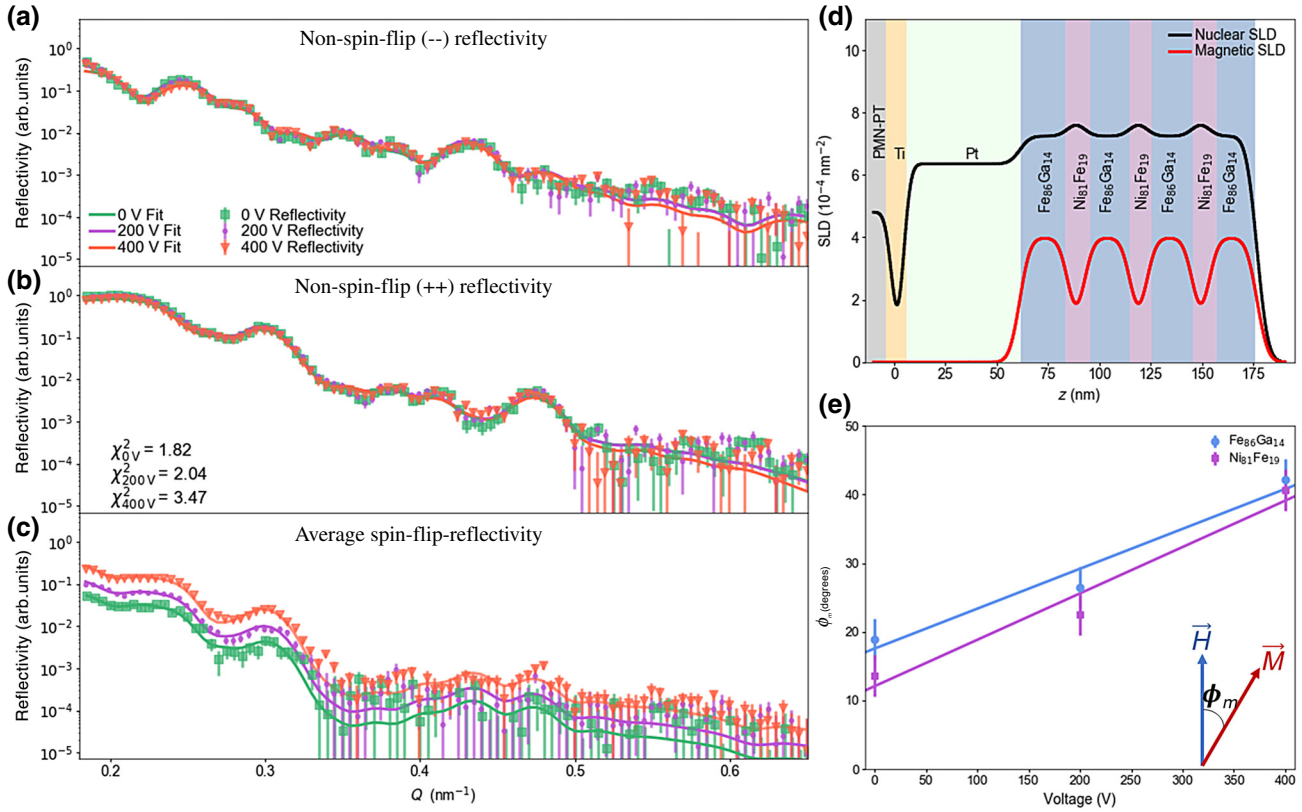


FIG. 2. PNR results for the superlattice. (a) Voltage-dependent non-spin-flip $R^{--}$, (b) non-spin-flip $R^{++}$, and (c) average of the spin-flip $R^{-+}$ and $R^{+-}$ (c). (d) Nuclear and magnetic SLD profiles determined from the fits in (a)–(c). (e) Angle between the applied field and the sample magnetization (shown in the inset) as determined from the fits. Error bars correspond to $\pm 1$ standard deviation for data and $\pm 2$ standard deviations for fitting parameters.

proceeds strictly through domain nucleation. However, while we can be certain that coherent rotation is the primary means of reversal, there is, of course, uncertainty in the modeling, meaning some small degree of nucleation is possible.

For this superlattice sample, the electric field is, in principle, coupled to the weakly magnetostrictive permalloy layers via strongly magnetostrictive galfenol layers dispersed throughout the structure. However, it remains unclear whether the magnetization of each individual galfenol layer rotates under the influence of a uniform magnetoelastic anisotropy dispersed through the thickness in response to a uniform stress. As discussed above, the voltage-induced lattice distortion may not be uniform throughout the sample thickness, raising the possibility that only a subset of the galfenol layers (perhaps only the one adjacent to the substrate) exhibits a magnetostrictive response, with the others rotating uniformly due to interlayer exchange coupling.

To isolate the role of exchange coupling and determine the extent over which it could be used to mediate coupling to the electric field, we examine the voltage-dependent magnetization in a bilayer sample with a thick (46-nm) permalloy layer anchored to the electric field by a single galfenol interface. Fitted PNR data for this bilayer are shown in Figs. 3(a)–3(c).

Again, $H$ is applied along the PMN-PT [100] direction. Similarly to the superlattice sample, there is relatively little voltage dependence for the non-spin-flip scattering, while the spin-flip scattering shows a significant increase with applied voltage.

The bilayer depth profile is shown in Fig. 3(d). Unlike the superlattice sample, the thicknesses are large enough that the fitted nuclear and magnetic SLD values for the galfenol and permalloy layers nearly match those expected for the bulk. As with the superlattice, we find that the bilayer data cannot be fitted to a model where the permalloy magnetization remains fixed with voltage [16], demonstrating that reversal again proceeds primarily through coherent rotation. However, we do find that some angular nonuniformity in the rotational depth profile of the bilayer does improve the fit. To gain some insight into what a physically realistic nonuniform rotation profile should look like across the thick permalloy layer, we perform micromagnetic simulations with the program MUMAX$^3$ [17]. We use a $500 \times 500 \times 60$ nm$^3$ array of spins discretized

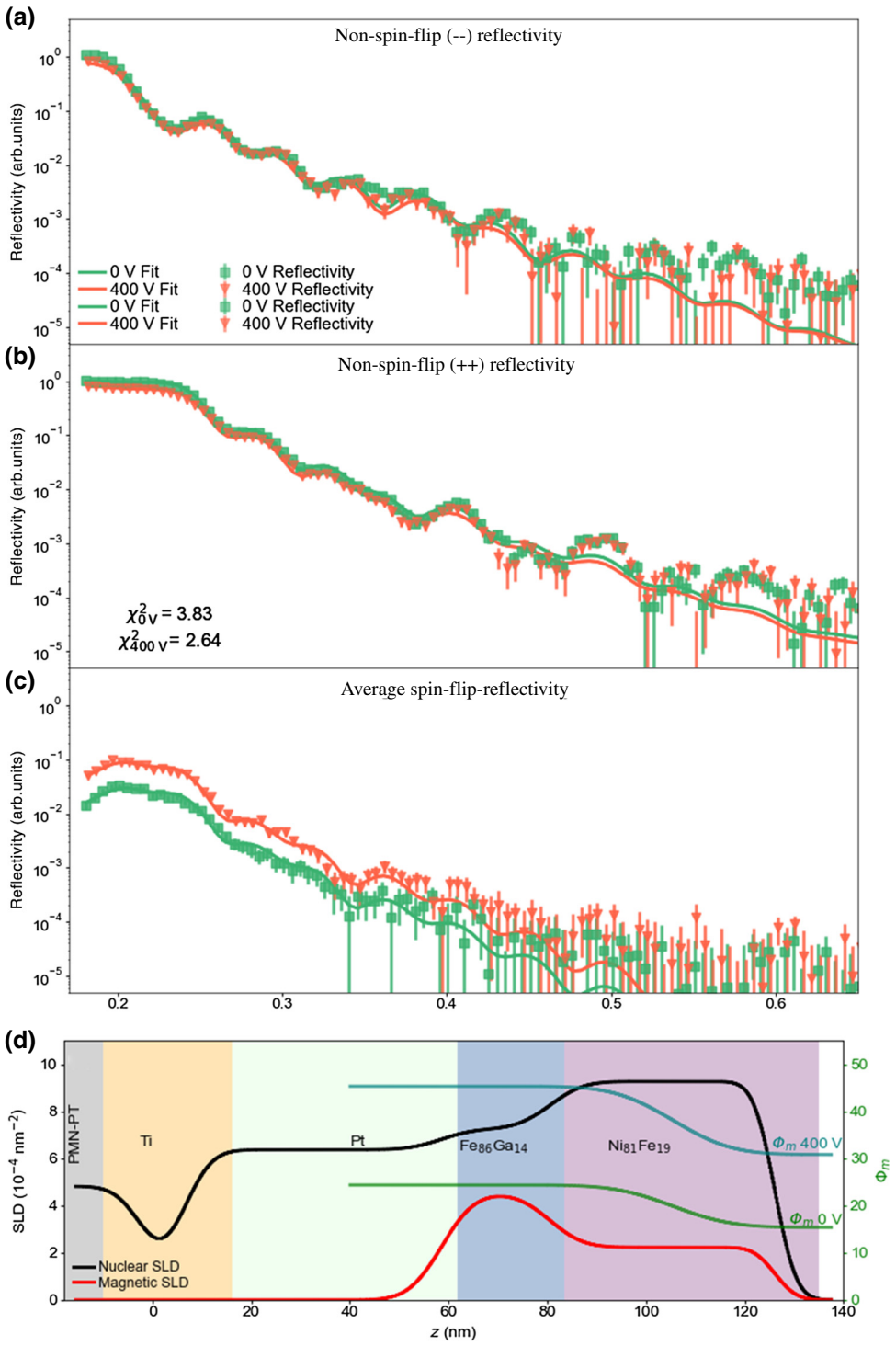


FIG. 3. PNR results for the 22-nm galfenol/46-nm permalloy bilayer. (a) Voltage-dependent non-spin-flip $R^{--}$, (b) non-spin-flip $R^{++}$, and (c) average of the spin-flip $R^{-+}$ and $R^{+-}$. (d) Nuclear and magnetic SLD profiles, along with the depth dependence of $\phi_m$ at 0 and 400 V, determined from the fits in (a)–(c). Error bars correspond to $\pm 1$ standard deviation.

into $2 \times 2 \times 1$ nm$^3$ cuboidal finite-difference-time-domain cells (a size chosen to be smaller than the exchange lengths of either material). To mimic the $1 \times 1$ cm$^2$ samples measured, periodic boundary conditions are applied until the model behavior converges to a thin-film limit. The bottom 20 nm of the magnetic volume is given the material properties of bulk amorphous $Fe_{86}Ga_{14}$ (saturation magnetization $M_S = 1300$ kA m$^{-1}$, exchange constant $A = 1.4 \times 10^{-11}$ J m$^{-1}$), while the top layer is given the properties of bulk $Ni_{80}Fe_{20}$ ($M_S = 860$ kA m$^{-1}$, $A = 1.3 \times 10^{-11}$ J m$^{-3}$). The two magnetic layers are initialized with their magnetizations aligned in plane. To simulate the response of permalloy to the voltage-induced rotation of galfenol, uniaxial anisotropy is applied to the $Fe_{86}Ga_{14}$ layer to rotate it by 90° in plane before the system is allowed to equilibrate for 1 ns. For these thicknesses, the

micromagnetic simulation predicts that even across 40 nm, the permalloy layer should rotate nearly coherently with a Gaussian-distributed angular profile that deviates by only 3° from the galfenol interface to the free surface (details are provided in Supplemental Material [16]).

With this in mind, the PNR data for the bilayer in Fig. 3 are fit to a model similar to that used for the superlattice, except that the permalloy magnetization rotation is allowed to vary smoothly (an error function). We constrain $\phi_m$ to be continuous at the galfenol/permalloy interface, and the nuclear SLD and the magnetic SLD are assumed to be voltage independent. The fits in Figs. 3(a)–3(c) are excellent below $Q \approx 0.45$ nm$^{-1}$, although they fall below the data at high $Q$. Variations of the model including both magnetic and structural nonuniformities cannot account for the high-$Q$ tail (or otherwise significantly improve the fit). We suspect instead that this discrepancy between data and simulation at high $Q$ can be attributed to the $Q$-dependent (i.e., incident-beam-angle-dependent) projection of the coherent extent of the neutron wavepacket onto the corrugated sample surface [18,19]. For our scattering geometry, this projection is a narrow stripe with the short axis parallel to $H$. At the lowest $Q$ measured, the projected area is approximately $75 \times 0.5$ $\mu$m$^2$, and is approximately $20 \times 0.5$ $\mu$m$^2$ at the highest $Q$. Since the ridges are narrow stripes approximately 50-$\mu$m wide that are tilted with respect to the beam direction, $Q \approx 0.45$ nm$^{-1}$ could correspond to a transition from neutrons scattering from individual structural domains (i.e., the ridges) to neutrons scattering from the average of multiple domains.

The best-fit profiles are shown in Fig. 3(d). Again, we see evidence of an easy-axis noncollinear with the direction of the applied magnetic field, with $\phi_m = 24°$ for galfenol at 0 V. The permalloy layer exhibits a 9° rotational gradient, with the magnetization aligned with that of galfenol at the galfenol interface, then decreasing to 15° (closer to alignment with $H$) at the free interface. Since permalloy is characteristically soft, the galfenol is likely the source of the magnetic anisotropy that gives rise to the in-plane easy axis at 0 V. On application of 400 V, the galfenol magnetization rotates an additional 21° away from the direction of the applied magnetic field to 45°, and the permalloy magnetization near the free surface rotates by 14° to 31°. Thus, the fitted permalloy gradient is 15° at 400 V. Overall, the profiles at 0 and 400 V should be interpreted as upper limits with regard to magnetic nonuniformity. While they do correspond to the best-fit parameters for this choice of model, a coherent model with $\phi_m$ of the galfenol and permalloy layers constrained to be equal provides a qualitatively similar fit to the data, as shown in Supplemental Material [16]. Importantly though, all of these models show that spins throughout the entire thickness of the permalloy layer respond to the electric field. Similar results are observed for nominally identical samples with thinner permalloy layers (7 and 20 nm) as detailed in Supplemental Material [16].

Overall, we observe significant voltage-induced magnetization rotation throughout permalloy layers as thick as 46 nm, a remarkable result considering that this distance is approximately an order of magnitude larger than the exchange length of permalloy (5 nm) [20].

## V. CONCLUSIONS

We use PNR to show that by exchange and strain coupling through a piezoelectric substrate and surrounding magnetostrictive layer(s), an applied electric field can be used to control the entire magnetization of thick (more than 100 nm) multiferroic composites with essentially nonmagnetostrictive permalloy layers. PNR measurements of a galfenol/permalloy bilayer allow us to isolate the role of interlayer exchange coupling, which we find to be remarkably long range. Micromagnetic calculations fully support these findings and imply a near-uniform manipulation of the magnetization is possible in even thicker structures. As such, we assert that designer galfenol/permalloy composite thin-film heterostructures are well positioned for imminent applications since electrical control of permalloy magnetization can be achieved over any practical length scales.

## ACKNOWLEDGMENTS

This work was supported by the NSF Nanosystems Engineering Research Center for Translational Applications of Nanoscale Multiferroic Systems under Cooperative Agreement Award No. EEC-1160504. This work made use of the University of California, Los Angeles, Integrated Systems Nanofabrication Cleanroom and the University of California, Los Angeles, Molecular Instrumentation Center. We thank T. Dax and Y. Kabanov of NIST for assistance with measurements, and D.A. Gilbert and R.D. Shull of NIST for helpful discussions.

[1] Ce-Wen Nan and M. I. Bichurin, Multiferroic magnetoelectric composites: Historical perspective, status, and future directions, J. Appl. Phys. **103**, 031101 (2008).

[2] Yao Wang, Jiamian Hu, Yuanhua Lin, and Ce-Wen Nan, Multiferroic magnetoelectric composite nanostructures, NPG Asia Mater. **2**, 61 (2010).

[3] Jing Ma, Jiamian Hu, Zheng Li, and Ce-Wen Nan, Recent progress in multiferroic magnetoelectric composites: From bulk to thin films, Adv. Mater. **23**, 1062 (2011).

[4] Jayasimha Atulasimha and Alison B. Flatau, A review of magnetostrictive iron-gallium alloys, Smart Mater. Struct. **20**, 043001 (2011).

[5] E. M. Sabolsky, A. R. James, S. Kwon, S. Trolier-McKinstry, and G. L. Messing, Piezoelectric properties of 001 textured $Pb(Mg_{1/3}Nb_{2/3})O_3$-$PbTiO_3$ ceramics, Appl. Phys. Lett. **78**, 2551 (2001).

[6] Shuxiang Dong, Junyi Zhai, Naigang Wang, Feiming Bai, JieFang Li, D. Viehland, and T. A. Lograsso, Fe–Ga/Pb($Mg_{1/3}Nb_{2/3}$)$O_3$–$PbTiO_3$ magnetoelectric laminate composites, Appl. Phys. Lett. **87**, 222504 (2005).

[7] Colin R. Rementer, Kevin Fitzell, Qiang Xu, Paul Nordeen, Gregory P. Carman, Yuanxun E. Wang, and Jane P. Chang, Tuning static and dynamic properties of FeGa/NiFe heterostructures, Appl. Phys. Lett. **110**, 242403 (2017).

[8] Tao Wu, Alexandre Bur, Ping Zhao, Kotekar P. Mohanchandra, Kin Wong, Kang L. Wang, Christopher S. Lynch, and Gregory P. Carman, Giant electric-field-induced reversible and permanent magnetization reorientation on magnetoelectric Ni/(011)[$Pb(Mg_{1/3}Nb_{2/3})O_3$]$_{(1-x)}$–[$PbTiO_3$]$_x$ heterostructure, Appl. Phys. Lett. **98**, 012504 (2011).

[9] C. F. Majkrzak, K. V. O'Donovan, and N. F. Berk, in *Neutron Scattering from Magnetic Materials* (Elsevier, New York, 2006), p. 397–471.

[10] B. J. Kirby, P. A. Kienzle, B. B. Maranville, N. F. Berk, J. Krycka, F. Heinrich, and C. F. Majkrzak, Phase-sensitive specular neutron reflectometry for imaging the nanometer scale composition depth profile of thin-film materials, Curr. Opin. Colloid Interface Sci. **17**, 44 (2012).

[11] As $R^{+-}$ and $R^{-+}$ are expected and observed to be identical, we show the average.

[12] Brian B. Maranville, Aaron Green, and Paul A. Kienzle, Distributed Error-Function Roughness in Refl1d Reflectometry Fitting Program, arXiv:1801.04975 [physics] (2017).

[13] M. R. Fitzsimmons and C. F. Majkrzak, in *Modern Techniques for Characterizing Magnetic Materials* (Springer, New York, 2005) p. 107.

[14] B. J. Kirby, J. W. Lau, D. V. Williams, C. A. Bauer, and Casey W. Miller, Impact of interfacial magnetism on magnetocaloric properties of thin film heterostructures, J. Appl. Phys. **109**, 063905 (2011).

[15] Zhe Guo, Xiaofei Yang, Xiangli Liu, Jun Ou-Yang, Benpeng Zhu, Shi Chen, and Yue Zhang, Electric field induced non-90° rotation of the easy axis of a ferromagnetic film, Appl. Phys. Lett. **112**, 052904 (2018).

[16] See Supplemental Material at http://link.aps.org/supplemental/10.1103/PhysRevApplied.10.044045 for information concerning the X-ray diffraction, optical profile of the PMN-PT, micromagnetic modeling details, and alternative fits to the PNR data.

[17] A. Vansteenkiste, J. Leliaert, M. Dvornik, M. Helsen, F. Garcia-Sanchez, and B. Van Waeyenberge, The design and verification of MuMax3, AIP Adv. **4**, 107133 (2014).

[18] Charles F. Majkrzak, Christopher Metting, Brian B. Maranville, Joseph A. Dura, Sushil Satija, Terrence Udovic, and Norman F. Berk, Determination of the effective transverse coherence of the neutron wave packet as employed inreflectivity investigations of condensed-matter structures. I. Measurements, Phys. Rev. A **89**, 033851 (2014).

[19] Lorenzo Fallarino, Brian J. Kirby, Matteo Pancaldi, Patricia Riego, Andrew L. Balk, Casey W. Miller, Paolo Vavassori, and Andreas Berger, Magnetic properties of epitaxial CoCr films with depth-dependent exchange-coupling profiles, Phys. Rev. B **95**, 134445 (2017).

[20] G. S. Abo, Y. K. Hong, J. Park, J. Lee, W. Lee, and B. C. Choi, Definition of Magnetic Exchange Length, IEEE Trans. Magn. **49**, 4937 (2013).